Unconventional cavity optomechanics: Nonlinear control of phonons in the acoustic quantum vacuum

Xin Wang [1,2] Wei Qin [2] Adam Miranowicz [2,3] Salvatore Savasta [2,4] and Franco Nori [2,5]

[1]*Institute of Quantum Optics and Quantum Information, School of Science, Xi'an Jiaotong University, Xi'an 710049, China*
[2]*Theoretical Quantum Physics Laboratory, RIKEN Cluster for Pioneering Research, Wako-shi, Saitama 351-0198, Japan*
[3]*Faculty of Physics, Adam Mickiewicz University, 61-614 Poznań, Poland*
[4]*Dipartimento di Scienze Matematiche e Informatiche, Scienze Fisiche e Scienze della Terra, Università di Messina, I-98166 Messina, Italy*
[5]*Physics Department, The University of Michigan, Ann Arbor, Michigan 48109-1040, USA*

We study unconventional cavity optomechanics and the acoustic analog of radiation pressure to show the possibility of nonlinear coherent control of phonons in the acoustic quantum vacuum. Specifically, we study systems where a quantized optical field effectively modifies the frequency of an acoustic resonator. We present a general method to enhance such a nonlinear interaction by employing an intermediate qubit. Compared to conventional optomechanical systems, the roles of mechanical and optical resonators are interchanged, and the boundary condition of the phonon resonator can be modulated with an ultrahigh optical frequency. These differences allow to test some quantum effects with parameters which are far beyond the reach of conventional cavity optomechanics. Based on this interaction form, we show that various nonclassical quantum effects can be realized. Examples include an effective method for modulating the resonance frequency of a phonon resonator (e.g., a surface-acoustic-wave resonator), demonstrating mechanical parametric amplification, and the dynamical Casimir effect of phonons originating from the acoustic quantum vacuum. Our results demonstrate that unconventional optomechanics offers a versatile hybrid platform for quantum engineering of nonclassical phonon states in quantum acoustodynamics.

I. INTRODUCTION

A. Conventional optomechanics

Optomechanical systems [1,2], in which quantized optical fields interact with a massive movable mirror via radiation pressure, bring together quantum physics and the macroscopic classical world. The basic mechanism of optomechanics is that the position of a movable mirror produces a time-dependent boundary condition of quantized electromagnetic fields, which, in turn, modulate an effective cavity resonant frequency [3]. Optomechanical systems provide a versatile platform to examine fundamental concepts of quantum physics and explore the classical-quantum boundary. Examples include testing wave-function-collapse models [4–6], studying the dynamical Casimir effect (DCE) [7–14], and putting massive objects into nonclassical states [15,16]. One may wonder whether there are unconventional optomechanical (UOM) systems where the *boundary condition of a mechanical resonator can be changed by a quantized optical field.* We show that such UOM systems can indeed exist, and give a general method to produce an UOM nonlinear interaction for controlling phonons (i.e., quantum engineering of phonons). In particular, we show how to realize a mechanical phase-sensitive amplifier and an acoustic analog of optical DCE. The acoustic DCE tries to simulate cosmological phenomena such as Hawking radiation and the Unruh effect [17–20]. However, no experiment has shown the phonon DCE using a phonon resonator at the quantum level, i.e., the effects where

quantized photons are converted into DCE pairs of itinerant phonons.

Let us recall the interaction form in a conventional optomechanical (COM) system. Setting $\hbar = 1$, an exact form of the interaction Hamiltonian between a single-mode optical field and a moving mirror is [3]

$$H_{\mathrm{COM}} = G_{\mathrm{COM}}(a + a^{\dagger})^2 (b + b^{\dagger}), \tag{1}$$

where a and b ($a^{\dagger}$ and $b^{\dagger}$) are the annihilation (creation) operators of the optical and mechanical modes, respectively and the single-photon coupling strength is G_{COM}. Note that in most studies the quadratic terms a^2 and $a^{\dagger 2}$ are often neglected because they describe rapidly oscillating virtual processes where photons are annihilated and created in pairs. As a result, the COM interaction

$$H'_{\mathrm{COM}} = 2G_{\mathrm{COM}} a^{\dagger} a (b + b^{\dagger}) \tag{2}$$

is obtained.

B. Main idea of proposed unconventional optomechanics

We start our discussion of an UOM system by considering a classical mechanical parametric amplifier (MPA), where the spring constant $k[E(t)]$ of a mechanical oscillator is modulated with a time-dependent field $E(t)$ [21–24]. As depicted in Fig. 1(a), we consider that the amplification source is not a classical drive, but a quantized electromagnetic field, $E(t) = \varepsilon_0 (a + a^{\dagger})$, oscillating at frequency ω_c, where ε_0 is
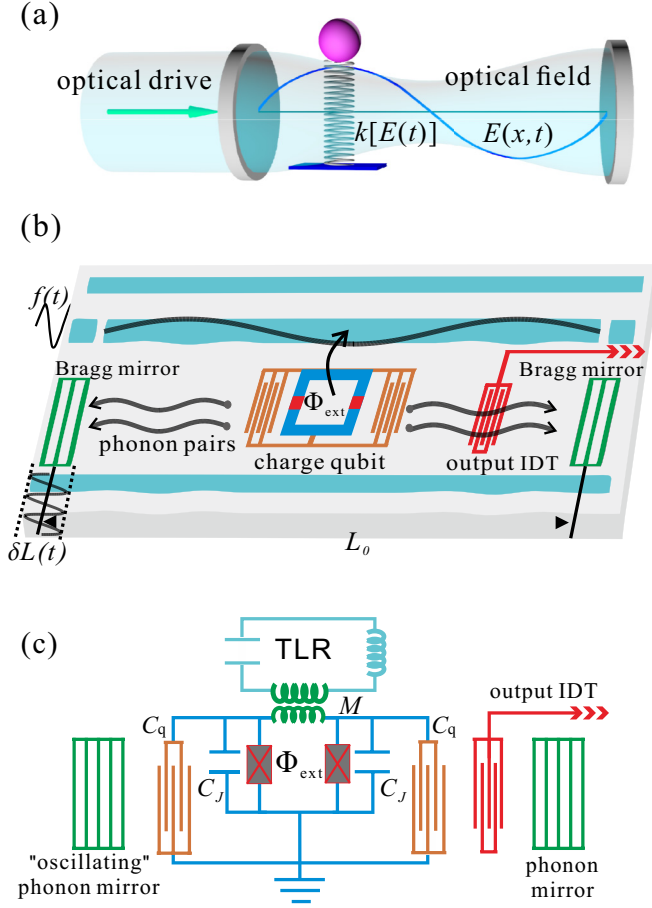
FIG. 1. (a) Diagrammatic sketch of an unconventional optomechanical (UOM) system: A localized mechanical oscillator (with a massive particle) is placed inside an optical cavity, and its spring constant is linearly modulated by the cavity field $E(x, t)$. (b) Schematic diagram and (c) lumped-circuit layout describing an unconventional optomechanical (UOM) system based on a surface-acoustic-wave (SAW) resonator: A charge qubit, with two Josephson junctions (red bars) is placed into the SAW resonator (confined by two Bragg mirrors). Their interaction is mediated via two identical inter-digitated-transducers (IDTs) of capacitance C_q via the piezoelectric effects. A transmission-line resonator (TLR) longitudinally couples to the charge qubit via the mutual inductance M. The UOM Hamiltonian in Eq. (5) can be mapped as the field current operator $\hat{I}(t)$ effectively changes the SAW resonator boundary condition. One Bragg mirror acts as a *fast "oscillating" mirror*.

the zero-point fluctuation. Expanding the potential term of the mechanical mode to first order in $E(t)$, we obtain the interaction term as [21]

$$V(t) = \tfrac{1}{2}k[E(t)]x^2 \simeq \tfrac{1}{2}k_0 x^2 + \tfrac{1}{2}RE(t)x^2, \quad (3)$$

where k_0 is the spring constant without the modulating field, and $x = x_0(b + b^\dagger)$ is the mechanical position operator with x_0 being the zero-point fluctuation. The last term in Eq. (3) describes the response of the spring constant to the optical field with sensitivity

$$R = \frac{\partial k(E)}{\partial E}\bigg|_{E=0}, \quad (4)$$

and can be rewritten as

$$H_{\text{UOM}} = G_{\text{UOM}}(b + b^\dagger)^2(a + a^\dagger), \quad G_{\text{UOM}} = \frac{R\varepsilon_0 x_0^2}{2}, \quad (5)$$

where G_{UOM} is the nonlinear coupling strength. Compared to the COM Hamiltonian, H_{UOM} has the inverse form, where the roles of the mechanical oscillator and optical field are interchanged.

We note that we are describing classical quantities using quantum-mechanical parameters, such as the creation and annihilation operators in Eqs. (1) and (2). Indeed, any classical system can be described using a quantum formalism. However, this does not mean that the reverse statement is true. A classical system would not be able to demonstrate a distinctly quantum performance in an experiment if the single-phonon coupling strength is suppressed by various kinds of decoherence processes. Moreover, ultraweak quantum coherent signals should be readout with reliable fidelities. In the following discussions, we will describe in detail methods which enable the observation of various quantum signatures of UOM systems.

The UOM interaction requires that the spring constant linearly responds to a fast-oscillating quantized electric field. To observe the coherence effects, this response should be ultrasensitive (a large R) to enable a strong coupling strength G_{UOM}. Obtaining such large R is still challenging in conventional MPA experiments. For example, in Ref. [24], the spring constant is modulated by an external voltage via the piezoelectric effect, and the sensitivity R is about 40 kHz/V. We assume that the external voltage is provided by a microwave transmission-line resonator (TLR), where the typical zero-point voltage fluctuation is ~ 0.1–$1 \, \mu$V [25]. The single-phonon UOM coupling strength is $G_{\text{UOM}} \simeq 10^{-2}$–$10^{-3}$Hz, which is too weak to produce observable coherent effects.

One can simulate the UOM interaction in a membrane-in-middle optomechanical system [26,27] based on the second-order optomechanical interactions and the semiclassical treatment of a cavity field. We stress that these membrane-in-the-middle configurations are still based on a COM system, which does *not interchange* the roles of phonons and photons. Thus the authors of Refs. [26,27] described only *simulations* of UOM-type interactions. In contrast to these works, our proposal describes *real* UOM with the *interchanged* roles of phonons and photons compared to COM. Our proposal is based on the first-order optomechanical interactions and the fully quantum treatment of the cavity field. Moreover, concerning the proposals in Refs. [26,27], no analogous phonon mirror can be found, and it is hard to control optical quantum fluctuations to reproduce (or simulate) a controllable boundary condition. Additionally, to avoid driving the system into the unstable and strongly squeezed regimes, the simulated interaction strength should be ultraweak. So far, no proposal has discussed how to realize a real UOM with strong-enough strength for quantum-optical engineering.

The paper is organized as follows: In Sec. II and Appendix A, we derive the basic qubit-mediated coupling for UOM. In Sec. III, we describe UOM based on hybrid superconducting circuits. In Sec. IV, we show a few examples of quantum control in UOM. These include modulating the frequency of a surface-acoustic-wave resonator (Sec. IV A),

quadratic coupling in UOM (Sec. IV B and Appendix B), and the phonon dynamical Casimir effect (Sec. IV C). We conclude in Sec. V.

II. QUBIT-MEDIATED COUPLING FOR UNCONVENTIONAL OPTOMECHANICS

Both optical and mechanical oscillators are linear bosonic systems. Single-phonon-photon nonlinear interactions (e.g., the COM coupling) are usually much weaker than conventional light-matter interactions [28,29]. To increase their nonlinear interactions, one possible method is to introduce nonlinear elements. For example, a Josephson-junction-based qubit can help to induce a strong COM interaction [30,31].

Concerning nonlinearity, a qubit is naturally a highly nonlinear system. By exploiting this nonlinearity, one may enhance the UOM interaction to an observable level. To introduce our idea, we consider a mechanical oscillator *transversely* interacting with a qubit with strength g_x. The optical cavity is involved in this hybrid system by its *longitudinal* coupling to the qubit with strength g_z [32–34]. By defining the qubit Pauli operators $\sigma_z = |e\rangle\langle e| - |g\rangle\langle g|$ and $\sigma_x = |e\rangle\langle g| + |g\rangle\langle e|$, where $|g\rangle$ and $|e\rangle$ are the qubit ground and excited states, the total Hamiltonian includes three parts, i.e.,

$$H_T = H_0 + H_1 + H_2, \tag{6a}$$

$$H_0 = \tfrac{1}{2}\omega_q \sigma_z + \omega_m b^\dagger b + \omega_c a^\dagger a, \tag{6b}$$

$$H_1 = g_z \sigma_z (a + a^\dagger), \tag{6c}$$

$$H_2 = g_x \sigma_x (b + b^\dagger). \tag{6d}$$

Here H_0 is the free Hamiltonian, with ω_q, ω_m, and ω_c being the qubit, mechanical resonator mode, and optical cavity mode eigenfrequencies, respectively; while H_1 and H_2 are the photon-qubit and phonon-qubit coupling Hamiltonians, respectively. The UOM interaction can be understood as follows: H_1 describes the quantized optical field operator $\xi = a + a^\dagger$, modulating the qubit frequency as

$$\omega_q(\xi) \longrightarrow \omega_q + 2g_z \xi.$$

Moreover, H_2 leads to a dispersive coupling between the qubit and the mechanical mode, i.e.,

$$H_{\text{dis}}(\xi) = \chi(\xi)(b^\dagger + b)^2 \sigma_z, \quad \chi(\xi) \simeq \frac{g_x^2}{\omega_q(\xi)}, \tag{7}$$

where the dispersive strength $\chi(\xi)$ is not a constant but depends on the field operator ξ. Different from the standard dispersive form, H_{dis} includes the additional quadratic terms $b^{\dagger 2}$ and b^2, which result from the counterrotating terms in H_2 [35]. Assuming that $\omega_q \gg \omega_m$, we approximately expand $H_{\text{dis}}(\xi)$ in ξ to obtain

$$H_{\text{dis}}(\xi) = \sum_{n=0}^{\infty} G_n \xi^n \sigma_z (b^\dagger + b)^2, \tag{8a}$$

$$G_n = \frac{1}{n!}\frac{\partial^n \chi(\xi)}{\partial \xi^n}\Big|_{\xi=0} \simeq (-1)^n \frac{g_x^2}{\omega_q^{n+1}}(2g_z)^n. \tag{8b}$$

Our detailed derivations are given in Appendix A. We assume that the qubit is initially in its ground state $|g\rangle$. Since the qubit is largely detuned from the mechanical mode, phonons

cannot effectively excite the qubit. Moreover, the longitudinal coupling commutes with the qubit operator σ_z, which does not cause any qubit state transition either. Therefore, it is reasonable to assume that the qubit is approximately in its ground state with $\langle \sigma_z \rangle \simeq -1$ in Eq. (8a). Under these conditions, the zeroth-order term can be reduced to

$$H_{\text{dis},0} = G_0 \sigma_z (b^\dagger + b)^2 \simeq -2G_0 b^\dagger b, \tag{9}$$

which shows that the mechanical frequency is renormalized as

$$\omega_m \longrightarrow (\omega_m - 2G_0). \tag{10}$$

The first- and second-order terms in Eq. (8a) describe the interaction between the mechanical oscillator and the optical field. The corresponding coupling ratio

$$\left|\frac{G_2}{G_1}\right| = \frac{2g_z}{\omega_q} \ll 1 \tag{11}$$

is a small parameter. Therefore, we just consider only the first-order term. Since the qubit degree of freedom is effectively eliminated, the Hamiltonian for the mechanical and optical modes can be written as

$$H_s \simeq \omega_c a^\dagger a + \omega_m b^\dagger b - G_1 (b^\dagger + b)^2 (a^\dagger + a). \tag{12}$$

Since the mechanical boundary condition is modulated with a fast-oscillating optical field, the quadratic terms b^2 and $b^{\dagger 2}$ in Eq. (5) cannot be dropped. To obtain an exact analog of H'_{COM}, one can employ a low-frequency optical resonator. Consequently, the rapidly oscillating terms, describing two-phonon processes, can be neglected. The UOM interaction can be reduced to

$$H'_{\text{UOM}} = 2G_1 b^\dagger b (a + a^\dagger). \tag{13}$$

As discussed in Appendix A, an alternative method is to shift the effective optical frequency via a parametric modulation of the longitudinal coupling [36,37]. Specifically, assuming that g_z is modulated at a frequency close to ω_c, the effective optical frequency $\omega'_c = (\omega_c - \omega_d)$ is shifted, becoming much smaller than ω_m. By controlling the modulating rate ω_d, the optical frequency ω_c is not fixed but tunable, which makes the UOM system more flexible. Therefore, the quadratic terms can also be safely neglected, thus, obtaining Eq. (13). Similar to the mechanism how radiation pressure acts on a macroscopic mirror [28], H'_{UOM} describes how *acoustic intensity* (or "phonon pressure" proportional to $\langle b^\dagger b \rangle$) *induces motions of the optical "position" operator* $(a + a^\dagger)$.

III. UNCONVENTIONAL OPTOMECHANICS BASED ON HYBRID SUPERCONDUCTING CIRCUITS

In the previous section, we showed how to obtain the UOM interaction by employing an intermediate qubit. Although such a method is very general and not specified to any certain quantum platform, we now give an example of UOM systems with a surface acoustic wave (SAW) resonator.

The majority of previous studies about various quantum features of phonons were demonstrated in localized mechanical resonators (MRs)(see, e.g., Refs. [38–41]), such as suspended cantilevers and doubly clamped MRs. In such systems, the size of the MRs is usually of the same order

of a phonon wavelength. Therefore, phonons spread through the whole volume of the MRs, thus it is not easy to observe phonon propagation in those nanoscale resonators. However, in the studies of SAWs, the piezoelectric surface behaves as an acoustic waveguide, and is usually much longer than the phonon wavelength [42,43]. As discussed in Refs. [44,45], the SAW propagation effects can be clearly observed and phonons can interact with atoms placed on their propagation paths. Due to these features, a SAW resonator can be employed as a quantum channel to mediate two artificial atoms for quantum information processing [44–46].

As shown in Fig. 1(b), phonons can be itinerant in a SAW resonator confined by two Bragg phonon mirrors [42,43,46–48]. Similar to an optical cavity, the Nth resonance acoustic mode depends on the phonon-mirror distance L_0 via the relation $\omega_m/(2\pi) = Nv_e/(2L_0)$, where v_e is the sound speed along the crystal surface. Here we consider a charge qubit [25] with two symmetric Josephson junctions (with Josephson energy E_J) placed inside the phonon resonator. The two junctions of the charge qubit form a superconducting quantum interference device (SQUID), and the total Josephson energy can be controlled via the external flux Φ_{ext} through it. The qubit capacitance C_q of an interdigitated-transducer (IDT) type shares the same periodicity with the resonator acoustic mode. The Hamiltonian for the charge qubit can be expressed as [25,49]

$$H_{\text{q}} = 4E_C(\hat{n} - n_g)^2 - 2E_J \cos\left(\frac{\pi \Phi_{\text{ext}}}{\Phi_0}\right) \cos\phi, \quad (14)$$

where $E_C = e^2/(2C_\Sigma)$ is the total charging energy of the two junctions and $C_\Sigma = C_J + C_g$ with C_J being the Josephson capacitance. To suppress the charge noise, one can apply a dc voltage to bias at the charge degeneracy point $n_g = 1/2$. The charge qubit Hamiltonian takes the form [25,50]

$$H_{\text{q}} \simeq -4E_C\delta n_g(|1\rangle\langle 1| - |0\rangle\langle 0|)$$
$$- E_J \cos\left(\frac{\pi \Phi_{\text{ext}}}{\Phi_0}\right)(|1\rangle\langle 0| + |0\rangle\langle 1|), \quad (15)$$

where $|0\rangle$ and $|1\rangle$ are the charge qubit states, and $\delta n_g = C_q V(t)/(2e)$ is the offset charge deviation from the optimal point, with $V(t)$ being the external voltage drive. The qubit capacitance C_q serves as a coupling element between the SAW resonator and the charge qubit. The interaction mechanism can be understood as follows: An acoustic wave travels on the crystal surface and generates an oscillating voltage $V(t)$ on the qubit capacitance C_q due to the piezoelectric effect [43]. Note that $V(t)$ is induced by the quantized motion and can be viewed as a time-dependent drive on the charge qubit. Although many discrete acoustic modes can, in principle, be excited in the phonon resonator, only one central mode is strongly coupled to the qubit [43]. Thus, it is physically justified to consider a single acoustic mode here. The voltage difference is associated with the zero-point mechanical fluctuation u_0 as $V(t) = u_0(b + b^\dagger)$. In the rotated basis with

$$|e\rangle = \frac{|1\rangle - |0\rangle}{\sqrt{2}}, \quad |g\rangle = \frac{|1\rangle + |0\rangle}{\sqrt{2}}, \quad (16)$$

the SAW-qubit coupling can be approximately written as [43]

$$H_{\text{qm}} = -4E_C\delta n_g\sigma_x = -\frac{eC_q}{C_\Sigma}u_0(b + b^\dagger)\sigma_x, \quad (17)$$

which corresponds to the transverse coupling between the SAW resonator and the charge qubit.

As depicted in Fig. 1(c), the effective Josephson energy depends on the external flux bias Φ_{ext}. One can couple the charge qubit with a TLR via a mutual inductance M. The central conductor of the TLR is along the x direction, and the interaction position is assumed to be at an antinode point of the current field $\hat{I}(x, t)$. The current $\hat{I} = I_0(a + a^\dagger)$ creates a flux perturbation

$$\delta\Phi_{\text{ext}} = MI_0(a + a^\dagger) \quad (18)$$

on the qubit static bias flux Φ_{ext}^0, where I_0 is the current zero-point-fluctuation amplitude, and a ($a^\dagger$) is the annihilation (creation) operator of the microwave photons. Therefore, we can expand the Josephson term in Eq. (15), to first order in $\delta\Phi_{\text{ext}}$, and obtain [51]

$$H_q = \frac{\omega_q}{2}\sigma_z + \frac{1}{2}\left(\frac{\partial\omega_q}{\partial\Phi_{\text{ext}}}\right)\Big|_{\Phi_{\text{ext}}^0}\sigma_z\delta\Phi_{\text{ext}}, \quad (19)$$

$$\omega_q = 2E_J\cos\left(\frac{\pi\Phi_{\text{ext}}}{\Phi_0}\right). \quad (20)$$

Note that the second term in Eq. (19) describes the interaction between the charge qubit and the TLR and can be written as

$$H_{\text{qc}} = g_z(a + a^\dagger)\sigma_z, \quad (21)$$

where the longitudinal coupling strength is

$$g_z = -\frac{\pi E_J}{\Phi_0}\sin\left(\frac{\pi\Phi_{\text{ext}}}{\Phi_0}\right)MI_0. \quad (22)$$

Up to now, we considered g_z to be a constant. A *parametrically modulated longitudinal coupling* between a superconducting qubit and a $\lambda/4$ (quarter wavelength) TLR can be realized by applying a time-dependent flux through the superconducting quantum interference device (SQUID) loop. A detailed description of the method can be found in Ref. [36].

In Refs. [43,48], the SAW resonator was assumed to couple with a transmon, and their coupling shared a similar expression as in Eq. (17) for the SAW-qubit coupling, except for a dimensionless parameter. The UOM interaction mediated by a transmon can also be produced. However, different from the charge qubit, a transmon is a weakly anharmonic system, and the UOM interaction based on a dispersive coupling (as described in Sec. II) will be disturbed by an imperfect state truncation at the first-excited level [52,53]. The UOM interaction in Eq. (8a) should be derived by considering higher-energy levels.

In addition to the SAW resonator, phonons can also exist in a localized MR. As discussed in Ref. [41], the transverse-coupling strength between a drum-type mechanical oscillator and a charge qubit can be engineered in the strong-coupling regime (about tens of MHz). By coupling the TLR (or LC resonator) quantized electromagnetic field with the split-junction loop of the charge qubit, the required longitudinal interaction can also be induced [51]. Therefore, one can realize the required Hamiltonian Eq. (6a), to generate the qubit-mediated

UOM interaction [Eq. (12)] for both SAW resonators and localized MRs.

IV. QUANTUM CONTROL IN UNCONVENTIONAL OPTOMECHANICS

The proposed UOM system differs from a COM system as follows. First, *the phonon-resonator boundary condition is modulated via a fast-oscillating optical field.* Therefore, we cannot drop the quadratic term (as we do for a COM system), which can induce observable quantum effects. Second, the COM Hamiltonian results from radiation pressure. However, the UOM interaction is mediated via a qubit and has no relation to moving the massive phonon mirrors via an optical (microwave) field. Indeed, it originates from a dispersive coupling being modulated by a quantized optical field. Due to these differences, the UOM interaction enables to observe some unconventional quantum phenomena. Below, by considering the SAW-resonator-based UOM system as an example, we show some possible quantum-control applications.

A. Modulating the frequency of a surface-acoustic-wave resonator

Using a large mutual inductance, the TLR-qubit interaction strength can easily enter into the strong- or even ultra-strong-coupling regimes [25,29]. The SAW-qubit coupling reaches tens of MHz in experiments [43,48]. By setting $g_x/(2\pi) = 60\,\text{MHz}$, $g_z/(2\pi) = 40\,\text{MHz}$, $\omega_q/(2\pi) = 3\,\text{GHz}$, and $\omega_m/(2\pi) = 250\,\text{MHz}$, one can obtain a single-phonon UOM coupling strength $G_1/(2\pi) \simeq -32\,\text{kHz}$, which is significantly enhanced compared to a direct coupling via the piezoelectric effect. We assume these values in our numerical calculations [54,55].

Analogously to COM, the optical field operator modifies the mechanical frequency as

$$\overline{\omega}_m = \sqrt{\omega_m^2 - 4G_1\omega_m\langle a^\dagger + a\rangle}. \tag{23}$$

To show this, we diagonalize Eq. (6a), and plot $(\overline{\omega}_m - \omega_m)$ versus $\langle\xi\rangle = \langle a^\dagger + a\rangle$ in Fig. 2(a). Clearly, the effective mechanical frequency is shifted away from ω_m by increasing $\langle\xi\rangle$. To derive H_{UOM} in Eq. (5), we just expand to first order in $\langle\xi\rangle$, by assuming $2g_z\langle\xi\rangle \ll \omega_q$. Therefore, our analytical formula for the shifted frequency slightly differs from the numerical results when $\langle\xi\rangle \gg 1$.

Note that the TLR can be replaced by a one-dimensional (1D) microwave guide [25], to which a classical microwave field can be applied. We assume that the current drive signal is

$$I(t) = \Theta(t)I_c, \tag{24}$$

where $\Theta(t)$ is the Heaviside unit step function, and I_c is the dc current strength applied to the 1D microwave guide when $t \geq 0$. The longitudinal coupling should be replaced with the classical step drive

$$H_\Theta = \Omega_s\sigma_z\Theta(t), \tag{25}$$

where

$$\Omega_s = -\frac{\pi E_J}{\Phi_0}\sin\left(\frac{\pi\Phi_{\text{ext}}}{\Phi_0}\right)MI_c. \tag{26}$$
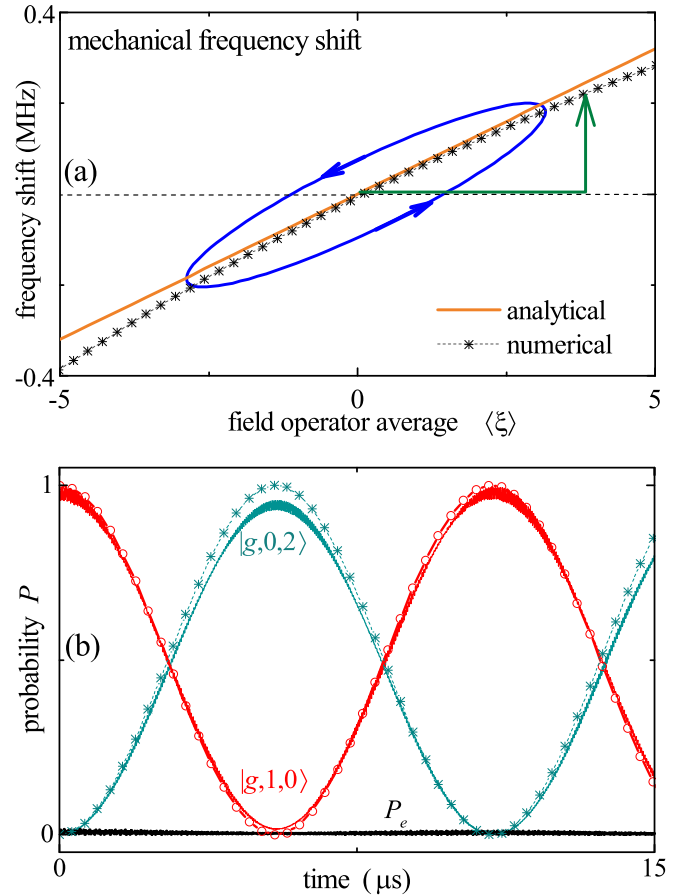

FIG. 2. (a) Mechanical frequency shift $(\overline{\omega}_m - \omega_m)$ versus the field operator average $\langle\xi\rangle = \langle a^\dagger + a\rangle$. The solid (asterisk) curve corresponds to the analytical (numerical) results. In numerical calculations, the shifted mechanical frequency is defined as the difference between the first and second eigenvalues in the subspace of the qubit ground state $|g\rangle$. The mechanical frequency can be suddenly (periodically) modulated via a step longitudinal bias (an oscillating electromagnetic field) along the green vertical arrow (the blue loop). (b) The Rabi oscillations between the states $|g, 0, 2\rangle$ and $|g, 1, 0\rangle$. The solid curves (symbols) represent the evolution described by the original Hamiltonian H_T (the reduced Hamiltonian H_Q). P_e is the probability of finding the qubit in its excited state.

Following the derivations in Sec. I and the discussions in Ref. [3], the interaction form corresponds to *changing the frequency and the length of the SAW resonator* at $t = 0$ with amounts

$$\delta\omega_m = \frac{4g_x^2}{\omega_q^2}\Omega_s, \quad \delta L = \frac{\delta\omega_m}{\omega_m}L_0, \tag{27}$$

respectively. Therefore, to effectively modify the resonance frequency of the SAW resonator, one can simply apply a current bias on the qubit longitudinal degree of freedom.

B. Quadratic coupling for mechanical parametric amplification

The phonon-resonator boundary condition in an UOM system is modulated by an optical field at an ultrahigh rate, which can easily exceed the phonon-resonator frequency. By setting

$\omega_c = 2\omega_m$, one can reduce H_{UOM} to a simpler Hamiltonian

$$H_Q = G_1(a^\dagger b^2 + ab^{\dagger 2}). \tag{28}$$

We denote $|g(e), n, m\rangle$ for the system containing n photons and m phonons, with the qubit in its ground (excited) state. The quadratic interaction H_Q can be verified clearly from Fig. 2(b), which shows the Rabi oscillations between the states $|g, 0, 2\rangle$ and $|g, 1, 0\rangle$ (solid curves, governed by H_T). The curves with symbols correspond to H_Q, which well match the exact results. During this photon-phonon conversion, the qubit-excited probability P_e oscillates with an ultralow amplitude above zero (the black curve). Thus we can safely neglect the qubit degree of freedom when deriving the effective UOM Hamiltonian. Note that H_Q can mimic the optomechanical quadratic interaction in a membrane-in-middle cavity system [26,56,57] with a much stronger strength (enhanced by the qubit). Therefore, various quantum-control applications, such as photon blockade and the generation of macroscopically distinct superposition state (Schrödinger cat-like states) [58–60], can be realized.

Given that the longitudinal drive of the qubit is

$$H_d = \Omega_d \sigma_z \cos(2\omega_m t + \phi), \tag{29}$$

we can approximately replace the field operator with a classical amplitude, i.e.,

$$a \to \alpha = \left(\frac{2g_x}{\omega_q}\right)^2 \Omega_d \exp(-i\phi). $$

When an ultraweak mechanical signal is injected into this UOM system, one quadrature X_{in} is amplified to an output X_{out} without introducing extra noise [61]. Note that the mechanism of an MPA based on a qubit-mediated UOM system is novel and different from that in conventional MPAs, where we should modulate in time the spring constant. In Appendix B, we derive the MPA gain as follows [62]:

$$G(\phi) = \left|\frac{X_{\mathrm{out}}}{X_{\mathrm{in}}}\right| = \frac{16|\alpha|^2 + \kappa^2 - 8|\alpha|\kappa \sin\phi}{16|\alpha|^2 - \kappa^2}. \tag{30}$$

In experiments, only some mechanical oscillators can be fabricated with a tunable spring constant [24]. Based on our proposed UOM mechanism, we find another general method for the MPA process by applying a longitudinal driving on the coupled qubit.

In Fig. 3, we plot G versus ϕ, and find that the gain reaches its maximum $G \simeq 14$ dB at $\phi = -\pi/2$. Different from an ideal MPA, there will be a qubit-induced Kerr nonlinearity. As discussed in Appendix B, once plenty of phonons are injected into the SAW resonator, the Kerr nonlinearity will destroy the amplifying process and drive the system out of the quasidispersive regime [63–65]. To avoid these undesired mechanisms, we require that the maximum phonon number satisfies Eq. (B9). Therefore, the maximum gain is bounded by

$$G_c \simeq (2N_c + 1)\left(1 + \sqrt{\frac{2N_c}{2N_c + 1}}\right)^2 \simeq (8N_c + 4). \tag{31}$$

Once the phonon number is beyond N_c, the qubit can be excited effectively, and the qubit-mediated UOM model is
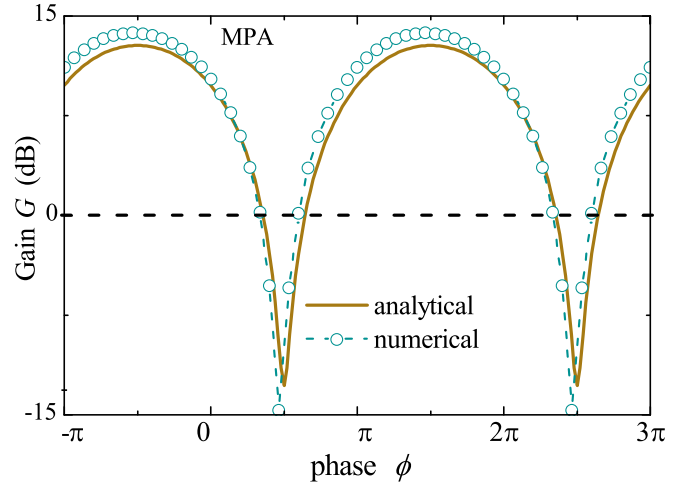

FIG. 3. The mechanical gain rate G of the input signals changing with the relative phase ϕ for MPA. The analytical results correspond to Eq. (30). We set $\alpha/(2\pi) = 0.045$ MHz. The qubit and phonon decay rates are $\Gamma/(2\pi) = 0.05$ MHz and $\kappa/(2\pi) = 0.2$ MHz, respectively.

not valid any more. However, even in our case with strong coupling strengths, the critical gain is still $G_c \simeq 29$ dB, below which one can safely amplify the mechanical signal for quantum measurements [58,62].

C. Phonon dynamical Casimir effect

Since the SAW frequency can be modulated by an optical field along the blue loop as shown Fig. 2(a) [3], one can alter the mode intensity of the *acoustic quantum vacuum* by the optical field [11]. Analogously to the optical DCE with an optomechanical system, in the following we describe the *phonon* DCE based on the UOM system [66,67].

As shown in Fig. 1(b), the interaction given by Eq. (12) can be interpreted as photons changing the effective distance L_0 between two phonon mirrors [3]. This indicates that the electromagnetic field can alter the mode intensity of the *phonon* field. Analogously to the photon dynamical Casimir effect (DCE) [9,10,68], phonon pairs are emitted due to the modulated-boundary condition of the *acoustic quantum vacuum*.

To verify this, we assume that the intracavity phonons can escape from the SAW resonator from an output channel. As shown in Fig. 1(c), one can employ an IDT to convert output phonons into electromagnetic signals (phonons) [43]. The boundary condition for the output field $c(t)$ and the intracavity SAW field $b(t)$ is

$$c(t) = b_{\mathrm{in}}(t) + \sqrt{\kappa}b(t), \tag{32}$$

where κ is the phonon escape rate from the SAW resonator and $b_{\mathrm{in}}(t)$ is assumed to be the vacuum input field. The output-phonon number per second is expressed as $P_{\mathrm{out}} = \kappa\langle c^\dagger c\rangle$. To describe the correlations between phonons, we define the second-order correlation function of the output field as

$$g_2(\tau) = \lim_{t \to \infty} \frac{\langle c^\dagger(t)c^\dagger(t + \tau)c(t + \tau)c(t)\rangle}{\langle c^\dagger(t)c(t)\rangle^2}, \tag{33}$$

with τ being the delay time. The phonon-flux spectrum density (detected by IDTs) is defined as

$$S(\omega) = \text{Re} \int_0^\infty \langle c^\dagger(0) c(\tau) \rangle e^{i\omega\tau} d\tau. \qquad (34)$$

We note that a phonon power spectrum can also be measured via electromotive techniques (see, e.g., Ref. [69] and reference therein). According to the Wiener-Khinchin theorem [70], and by replacing the output operator with the intracavity field, one can find that

$$S(\omega) \propto n_{\text{out}}(\omega) = \int_0^\infty \text{Tr}[\rho b^\dagger(\omega) b(\omega')] d\omega', \qquad (35)$$

where

$$b(\omega) = \frac{1}{\sqrt{2\pi}} \int_{-\infty}^\infty b(t) e^{-i\omega t} dt \qquad (36)$$

is the Fourier transform of the intracavity field operator $b(t)$, and satisfies the canonical commutation relation

$$[b(\omega), b^\dagger(\omega')] = \delta(\omega - \omega'). \qquad (37)$$

Assuming that the TLR is resonantly driven via a coherent field with strength ϵ, i.e.,

$$H_d(t) = \epsilon[a \exp(i\omega_c t) + a^\dagger \exp(-i\omega_c t)]. \qquad (38)$$

We numerically simulate the quantum evolution of the system described by the Lindblad-type master equation

$$\frac{d\rho(t)}{dt} = -i[H_1 + H_d(t), \rho(t)] + \Gamma D[\sigma_-]\rho(t) + \gamma D[a]\rho(t)$$

$$+ \kappa n_{\text{th}} D[b]\rho(t) + \kappa(n_{\text{th}} + 1)D[b^\dagger]\rho(t), \qquad (39)$$

where Γ, γ, and κ are the decay rates for the qubit, optical resonator, and SAW resonator, respectively, n_{th} is the thermal phonon number, and

$$D[A]\rho = (2A\rho A^\dagger - A^\dagger A\rho - \rho A^\dagger A)/2 \qquad (40)$$

is the decoherence term in the Lindblad superoperator form. Note that we consider the original Hamiltonian H_T, given in Eq. (6a) (including the qubit degree of freedom), rather than the reduced UOM Hamiltonian H_s, given in Eq. (12).

We first consider the SAW resonator coupled to a zero-temperature reservoir ($n_{\text{th}} = 0$). As predicted in the optical DCE, with increasing the drive strength ϵ, the effective length of the SAW resonator is modulated with a higher amplitude. In Fig. 4(a), by setting $\omega_c = 2\omega_m$, we plot the phonon output rate P_{out} changing with ϵ. We find that, with large ϵ, P_{out} is enhanced. At $\epsilon/(2\pi) = 0.05$ MHz (dashed line), the output phonon number per second is about $P_{\text{out}} \simeq 1 \times 10^5$, which can be effectively detected by an IDT measurement [48].

Since there are no thermal excitations and no coherent drive applied to the SAW resonator, these phonons might be generated by the phonon DCE, and have the same quantum signatures as photons generated in the optical DCE. As discussed in Refs. [10,71], the DCE excitations are created in pairs. To show this, in Fig. 4(a), we plot the second-order correlation function $g_2(0)$ as a function of the TLR drive strength ϵ. We find that the generated phonons have super-Poissonian phonon-number statistics with $g_2(0) \gg 2$. When ϵ has ultralow amplitude, $g_2(0)$ becomes infinitely large [68].
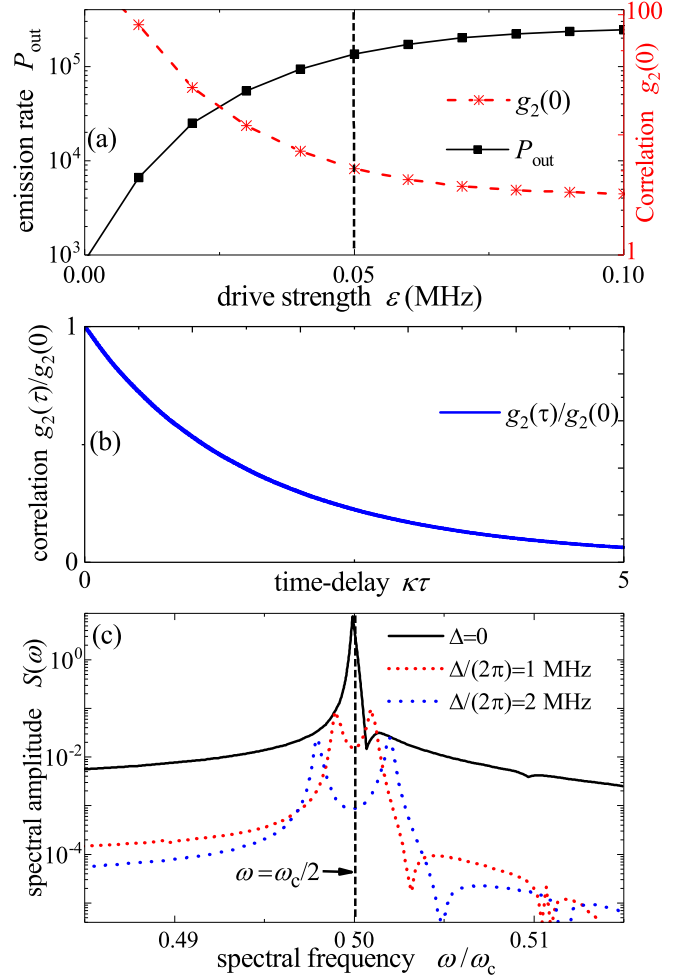

FIG. 4. (a) Phonon-output rate P_{out}, and correlation function $g_2(0)$, as functions of the TLR drive strength ϵ. The dashed line is plotted at $\epsilon/(2\pi) = 0.05$ MHz, which is set in plots (b) and (c). (b) Normalized correlation function $g_2(\tau)/g_2(0)$ changing with the delay time $\kappa\tau$. (c) Phonon output spectrum density $S(\omega)$, for different detuning cases. The dotted line position corresponds to $\omega = \omega_c/2$. Here the decay rates are $\Gamma/(2\pi) = 0.05$ MHz, $\kappa/(2\pi) = 0.2$ MHz, and $\gamma/(2\pi) = 0.1$ MHz.

Due to the increasing phonon intensity [13], $g_2(0)$ decreases with increasing the drive strength. Moreover, in Fig. 4(b), we plot the normalized correlation function $g_2(\tau)/g_2(0)$ changing with the delay time $\kappa\tau$. We find that $g_2(0) \gg g_2(\tau)$, indicating that the emitted phonons exhibit strong bunching, which is due to the same mechanism as that in the optical DCE [68].

In Fig. 4(c), we plot the spectrum density $n_{\text{out}}(\omega)$ for different values of the detuning $\Delta_d = \omega_c - 2\omega_m$. When $\Delta_d = 0$, the phonon-flux density spectrum shows a single-peak at $\omega = \omega_s/2$. When $\Delta_d \neq 0$, $n_{\text{out}}(\omega)$ shows a clearly symmetric bimodal spectrum at ω' and ω'', with $\omega' + \omega'' = \omega_c$, which is another strong indication of the phonon DCE [72]. Compared to the resonance case, the correlated emitted phonon pairs are not degenerate any more, but distributed into two conjugate modes with different frequencies. When increasing the detuning Δ_d, the peaks of two modes separate with larger distance, while the amplitudes are suppressed significantly.

As discussed in Sec. II, the TLR can be replaced by a 1D transmission waveguide, which can support a classical drive current. Equations (26) and (27) indicate that the pulse shape in the waveguide directly determines how the effective phonon resonator length changes with time. We consider a simple case where a sinusoidal current pulse

$$I(t) = \Theta(t) I_c \cos(\Omega t)$$

is applied, which is equal to a coherent drive on the qubit operator σ_z with strength $\Omega_d = g_z I_c / I_0$. Following Eq. (27), *the current produces a time-dependent modulation of the effective phonon resonator length*

$$\delta L(t) = \frac{4 g_x^2}{\omega_q^2} \frac{\Omega_d}{\omega_m} L_0 \cos(\Omega t). \tag{41}$$

The sinusoidal modulation can be mapped as *moving a phonon mirror with a nonuniform acceleration* [11]. Similarly, we can observe the *phonon DCE*. In the following, we consider how a nonzero temperature phonon reservoir influencing the *phonon* DCE signals. Compared to photons, phonons are much more fragile to environmental noise. Thus, their generation and detection processes should be considered carefully. Specifically, the DCE signals should be distinguished from thermal excitations and other kinds of noise. In the following discussions, we present methods to identify the DCE phonons from the sea of noisy thermal phonons.

As shown in Fig. 1(b), the phonons in the SAW resonator can be collected by the output IDT channel. Once considering thermal effects, the emitted phonons from the SAW resonator can be divided into two types: the DCE-induced phonon pairs and thermalized incoherent phonons.

One can define the signal-to-noise-ratio (SNR) of the DCE as

$$\text{SNR} = \frac{P_{\text{out}} - P_{\text{out}}^{\text{th}}}{P_{\text{out}}^{\text{th}}}, \tag{42}$$

where $P_{\text{out}}^{\text{th}}$ is the output *phonon* rate without modulating the effective resonator length, and P_{out} is the total output phonon rate. Therefore, $P_{\text{out}}^{\text{th}}$ corresponds to purely thermal excitations and should be considered as a noise contribution. In Fig. 5(a), by setting $\Omega = 2\omega_m$, we plot the SNR of the DCE versus the environment temperature T. We find that the SNR decreases quickly with increasing temperature. When $T > 27$ mK, the SNR is below 1, indicating that the DCE signal is hidden in the noisy background.

In addition to employing the output power to confirm the DCE phonons, we can detect their quantum correlations. As discussed before, the DCE phonons are generated in pairs. Therefore, their second-order correlation function $g_2(0)$ is super-Poissonian, and much higher than that of thermal excitations. In Fig. 5(a), we plot $g_2(0)$ versus temperature T. We find that $g_2(0)$ is very large, with $g_2(0) \gg 2$ in the limit of $T \to 0$. When $T \simeq 50$ mK, the DCE phonons are significantly polluted by thermal excitations, and the output correlation function $g_2(0) \simeq 2$ is almost the same as that for genuine thermal noise. The numerical results shown in Fig. 5(a) indicate that the DCE signal can be well separated from thermal noise given that the environment temperature is below $T \simeq$
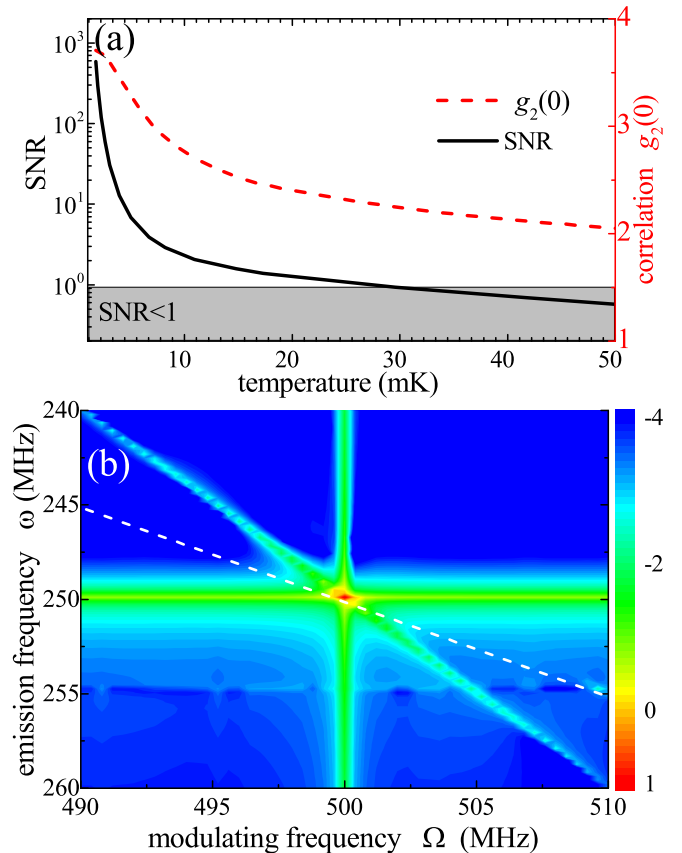

FIG. 5. (a) Signal-to-noise-ratio (SNR) and second-order correlation function $g_2(0)$ versus the thermal phonon number n_{th}. The gray area corresponds to SNR < 1. (b) The emitted phonon spectrum $\log[S(\omega)]$ changes with the modulating frequency Ω. A bimodal spectrum structure distributes along the dashed line (which corresponds to $\omega = \Omega/2$). Here we set the coherent drive amplitude on the qubit as $\Omega_d/(2\pi) = 100$ MHz. Other parameters are the same as those in Fig. 4.

20 mK. The hybrid quantum circuits based on SAWs are usually placed in diluted refrigerators, in which the temperature $T \simeq 20$ mK is achievable [25,73]. At temperatures of tens of mK, the quantum manipulating and topography measurement of propagating SAW phonons have been realized experimentally [43,44,48,73]. Therefore, we believe that the observation of these quantum signatures of DCE phonon pairs is possible using current experimental approaches.

In Fig. 5(b), by setting $n_{\text{th}} = 0.02$, we plot the emission spectrum $S(\omega)$ changing with the coherent modulation frequency Ω. The dashed line position is plotted for $\omega = \Omega/2$. The bimodal structure of the emission spectrum is still kept. However, due to thermal noise, the two peaks are not symmetric any more. To suppress the effect of thermal noise on the DCE signals, one can employ high-frequency modes of the SAW cavity. As discussed in the experiments reported in Refs. [42,43,48], the SAW resonance frequency can be engineered for about several GHz, and the thermal occupation number n_{th} can be below 10^{-3} at temperatures ~ 20 mK, which is within the capability of up-to-date hybrid quantum circuit implementations in dilution refrigerators.

In Fig. 2(b), the time-dependent evolutions indicates that there is the vacuum Casimir-Rabi coupling in UOM systems [13], and we can the observe the phonon DCE in an UOM system. Figure 4(c) is also another strong indication of the *phonon DCE* where excitations are created in pairs [Fig. 1(b)]. Compared to the resonance case, the emitted phonon pairs in the detuning case are not degenerate any more, but distributed into two conjugate modes with different frequencies.

To observe the *optical DCE* (i) the mechanical mode should oscillate at an ultrahigh frequency (corresponding to moving the mirror near the speed of light, instead of the speed of sound for the phonon case), and (ii) a strong optomechanical interaction should be induced [9–11]. Both requirements are exceedingly challenging in experiments. So far, no experiment has successfully demonstrated a real optical DCE involving the mechanical-optical energy conversion [13]. However, the *phonon DCE* described here is much easier to induce and observe since the boundary condition is modulated by a microwave field: The electromagnetic frequency can easily overwhelm the phonon resonator frequency. Moreover, a strong mechanical-optical UOM coupling, which is enhanced by the intermediate qubit, enables observing the phonon DCE at the quantum level.

V. CONCLUSION

We propose an UOM mechanism, which describes how the frequency of a mechanical mode is effectively modulated by a quantized optical field. We present a general method to enhance the UOM coupling via an intermediate qubit. For example, by considering a SAW resonator, we find that the effective resonator length is not fixed, but can be shifted in a large range by simply applying a longitudinal bias on the qubit, which allows more controllability in SAW-resonator experiments. In principle, analogs of various quantum effects studied in COM, can be demonstrated in UOM systems, but with the interchanged roles of photons and phonons. Recently, quantum acoustodynamics has emerged as a powerful platform to explore quantum features of acoustic waves. The UOM mechanism allows to manipulate itinerant phonons at the quantum level [42,43,47,48,74]. For example, an UOM system can serve as a *nonlinear transducer converting quantum information between acoustic waves and microwave resonators*. Other examples include mechanical phase-sensitive amplification and phonon DCE. We hope that other quantum mechanisms and applications can be developed in UOM systems in future studies.

APPENDIX A: UNCONVENTIONAL OPTOMECHANICAL HAMILTONIAN

We now present detailed derivations of unconventional cavity optomechanics (UOM) mediated by a qubit. We start our discussions by first considering a mechanical oscillator interacting with a qubit with strength g_x, i.e.,

$$H_{qm} = \tfrac{1}{2}\omega_q \sigma_z + \omega_m b^\dagger b + g_x \sigma_x (b^\dagger + b), \quad (A1)$$

where b ($b^\dagger$) are the annihilation (creation) operators of the mechanical mode, ω_q is the qubit transition frequency, while $\sigma_z = |e\rangle\langle e| - |g\rangle\langle g|$ and $\sigma_x = |e\rangle\langle g| + |g\rangle\langle e|$ are the qubit Pauli operators with $|e\rangle$ ($|g\rangle$) being the excited (ground) state. We assume that the system is largely detuned with $(\omega_q - \omega_m) \gg g_x$. The optical cavity is involved in this bipartite system by considering its longitudinal coupling with the qubit [32–34,75], which is described by the Hamiltonian

$$H_{qc} = g_{z0} \cos(\omega_d t)\sigma_z(a^\dagger + a), \quad (A2)$$

where a ($a^\dagger$) are the annihilation (creation) operators of the optical mode. As in Ref. [36], we consider a general case, where the *longitudinal coupling* g_{z0} is *parametrically modulated* at a frequency ω_d. Note that the following discussions can also be applied to the constant longitudinal case. Consequently, the system Hamiltonian becomes

$$H_0 = \tfrac{1}{2}\omega_q \sigma_z + \omega_{c0} a^\dagger a + \omega_m b^\dagger b$$
$$+ g_{z0}\cos(\omega_d t)\sigma_z(a^\dagger + a) + g_x \sigma_x(b^\dagger + b), \quad (A3)$$

where ω_{c0} is the resonator frequency. By rotating the resonator at frequency ω_d, and neglecting the rapidly oscillating terms, we obtain

$$H_1 = \frac{\omega_q}{2}\sigma_z + \omega_c a^\dagger a + \omega_m b^\dagger b + g_z \sigma_z(a^\dagger + a) + g_x \sigma_x(b^\dagger + b), \quad (A4)$$

where $\omega_c = \omega_{c0} - \omega_d$ is the shifted resonator frequency and $g_z = g_{z0}/2$ is an effective longitudinal coupling strength. Later we find that this modulation allows us to obtain an exact analog of the conventional optomechanical Hamiltonian by dropping the quadratic terms.

By setting $\xi = (a^\dagger + a)$, the longitudinal interaction can be viewed as the quantized optical field modulating the qubit transition frequency as

$$\omega_q(\xi) = \omega_q + 2g_z \xi.$$

Here we assume that the qubit-mechanical interaction is in the dispersive regime. By defining

$$X_\pm = \sigma_- b^\dagger \pm \sigma_+ b, \quad Y_\pm = \sigma_+ b^\dagger \pm \sigma_- b, \quad (A5)$$

we can rewrite H_1 as

$$H_2 = \tfrac{1}{2}\omega_q(\xi)\sigma_z + \omega_c a^\dagger a + \omega_m b^\dagger b + g_x(X_+ + Y_+). \quad (A6)$$

Different from the standard derivations of dispersive coupling under the rotating wave approximation, we also consider the counterrotating term Y_+ in H_2. Applying the unitary transformation [35]

$$U = \exp[\lambda_-(\xi)X_- + \lambda_+(\xi)Y_-], \quad \lambda_\pm(\xi) = \frac{g_x}{\omega_q(\xi) \pm \omega_c},$$
(A7)

to H_2, we can expand the transformed Hamiltonian $\widetilde{H} = U^\dagger H_2 U$ to first order in the small parameters $\lambda_\pm(\xi)$. Thus, we obtain the following dispersive-type coupling Hamiltonian:

$$\widetilde{H} \simeq H_0 + H_{\text{dis}},$$
(A8)

$$H_0(\xi) = \frac{\omega_q(\xi)}{2}\sigma_z + \omega_c a^\dagger a + \omega_m b^\dagger b,$$
(A9)

$$H_{\text{dis}}(\xi) = \frac{1}{2}\sigma_z g_x[\lambda_+(\xi) + \lambda_-(\xi)](b^\dagger + b)^2.$$
(A10)

Comparing to the standard dispersive coupling, we find two differences in Eq. (A10). First, due to counterrotating contributions, the quadratic terms b^2 and $b^{\dagger 2}$ are also involved. Second, more importantly, the dispersive coupling strength

$$\chi(\xi) = \frac{1}{2}g_x[\lambda_+(\xi) + \lambda_-(\xi)] = \frac{g_x^2\,\omega_q(\xi)}{\omega_q^2(\xi) - \omega_m^2}$$
(A11)

is not constant but depends on the quantized optical field operator $\xi = a + a^\dagger$. Assuming that $\omega_q \gg 2g_z\xi$ and $\omega_q \gg \omega_m$, we approximately expand $H_{\text{dis}}(\xi)$ to second order in ξ, and obtain Eq. (8).

Given that

$$\delta_s = (\omega_c - 2\omega_m) \gg G_1,$$
(A12)

the interaction Hamiltonian in Eq. (12) reads

$$H_\delta = G_1[a^\dagger b^2 \exp(i\delta_s t) + ab^{\dagger 2}\exp(-i\delta_s t)],$$
(A13)

from which we can obtain the cross-Kerr interaction between these two modes [76], i.e.,

$$H_{\text{ck}} = \frac{2G_1^2}{\delta_s}[a^\dagger a(2b^\dagger b + 1) - b^{\dagger 2}b^2].$$
(A14)

This interaction describes that the average phonon number operator $\langle n \rangle = \langle b^\dagger b \rangle$, will effectively shift the optical frequency. Equation (8a) also contains a cross-Kerr coupling with strength $-2G_2$ (a second-order term). Therefore, the phonon number $\langle n \rangle = \langle b^\dagger b \rangle$ eventually shifts the optical frequency by the amount

$$\delta\omega_c = \chi_k\langle n \rangle, \quad \chi_k = \left[\frac{4G_1^2}{\delta_s} - 2G_2\right].$$
(A15)

By setting $\delta_s = 20G_1$ and adopting the parameters specified in the main article, the optical frequency shift per phonon is about $\chi_k/(2\pi) \simeq -10\,\text{kHz}$. Since H_{ck} commutes with the phonon-number operator, this interaction can be employed for phonon quantum nondemolition (QND) measurements and phonon distribution counting [76,77].

Finally, we discuss the parameter regimes where this qubit-mediated coupling for unconventional cavity optomechanics (UOM) is valid. First, we recall that the effective interaction is based on the dispersive coupling between the mechanical

mode and the qubit, which sets a limitation on the average phonon number as [25]

$$\langle n \rangle = \langle b^\dagger b \rangle \leqslant \frac{1}{(2\lambda_-)^2}.$$
(A16)

Second, the convergence of the expansion, given in Eq. (8b), requires that $\langle \xi \rangle \leqslant 2g_z/\omega_q$, which also sets a bound for the optical intracavity field amplitude.

APPENDIX B: MECHANICAL PARAMETRIC AMPLIFIER BASED ON UNCONVENTIONAL OPTOMECHANICS

In Fig. 1(b), the TLR can be replaced by a 1D microwave guide, which allows for a classical current signal to propagate inside. As a result, the shape of the classical drive applied to the qubit directly determines the boundary condition of the SAW resonator. Here we consider the UOM system working as a phase-sensitive mechanical parametric amplifier (MPA) [21,22], which can enhance one quadrature of an ultraweak mechanical signal for quantum detection. To this end, we assume that the longitudinal drive of the qubit has the form

$$H_d = \Omega_d\sigma_z\cos(2\omega_m t + \phi).$$
(B1)

Following the derivation steps in Sec. I, the effective Hamiltonian reads

$$H_{\text{MPA}} = \alpha b^{\dagger 2} + \alpha^* b^2,$$
(B2)

$$\alpha = \Omega_d\frac{g_x^2(\omega_q^2 + \omega_m^2)}{(\omega_q^2 - \omega_m^2)^2}e^{-i\phi} \simeq \Omega_d\left(\frac{g_x}{\omega_q}\right)^2 e^{-i\phi}.$$
(B3)

Since the qubit is a highly nonlinear system, it introduces a Kerr nonlinearity in the SAW resonator [65], i.e.,

$$H_k = K(b^\dagger b^\dagger bb)\sigma_z, \quad K = \frac{g_x^4}{\omega_q^3}.$$

We consider that a weak mechanical signal is injected into the SAW resonator, i.e.,

$$H_{\text{in}} = i\sqrt{\kappa}(c_{\text{in}}^\dagger b - c_{\text{in}}b^\dagger),$$

where κ is the phonon damping rate of the input channel, and c_{in} is the input field operator. The output signal c_{out} can be obtained via the input-output relation

$$c_{\text{out}}(t) = \sqrt{\kappa}b(t) + c_{\text{in}}.$$

The Heisenberg equation for the phonon operator $b(t)$ reads

$$\dot{b}(t) = -2i\alpha b^\dagger(t) - \frac{\kappa}{2}b(t) - 2iKN(t)\sigma_z(t)b(t) - \sqrt{\kappa}c_{\text{in}},$$
(B4)

where $N(t) = \langle b^\dagger(t)b(t) \rangle$ is the mean phonon number. We define the input (output) quadratures

$$X_{\text{in,out}} = \frac{c_{\text{in,out}}^\dagger + c_{\text{in,out}}}{\sqrt{2}}, \quad Y_{\text{in,out}} = \frac{i(c_{\text{in,out}}^\dagger - c_{\text{in,out}})}{\sqrt{2}}.$$
(B5)

As we discussed in Sec. I, the qubit is approximately in its ground state. Therefore, we set $\sigma_z = -1$ and obtain

$$\dot{X}(t) = -\frac{1}{2}\kappa X(t) - 2KN(t)Y(t)$$
$$- 2|\alpha|[\cos\phi Y(t) + \sin\phi X(t)] - \sqrt{\kappa}X_{\text{in}}, \quad \text{(B6)}$$

$$\dot{Y}(t) = -\frac{1}{2}\kappa Y(t) + 2KN(t)X(t)$$
$$+ 2|\alpha|[\cos\phi X(t) + \sin\phi Y(t)] - \sqrt{\kappa}Y_{\text{in}}, \quad \text{(B7)}$$

where

$$X = \frac{b^\dagger + b}{\sqrt{2}}, \quad Y = \frac{i(b^\dagger - b)}{\sqrt{2}} \quad \text{(B8)}$$

are the intracavity quadratures. We assume that the quadrature X_{in} is to be amplified and satisfies the boundary relation $X_{\text{out}} = \sqrt{\kappa}X + X_{\text{in}}$. From Eq. (B7) one can find that, only under the conditions $\cos\phi = 0$ and $K = 0$, the evolutions of the quadratures X and Y are decoupled, and one can amplify X_{in} independently [62]. The Kerr nonlinearity couples both quadratures and should be avoided. In experiments, K cannot be exactly equal to zero. To minimize the effects of the quadrature Y on X, we require that the induced Kerr nonlinearity term satisfies $KN(t) \ll |\alpha|$, which leads to

$$N \ll \frac{|\alpha|}{K} \simeq \frac{\Omega_d\omega_q}{g_x^2}. \quad \text{(B9)}$$

Therefore, the qubit-induced Kerr nonlinearity sets an upper bound of the mean phonon number, below which one can safely neglect the Kerr terms in Eqs. (B6) and (B7). We consider that the amplification process works below the threshold regime ($2|\alpha| < \kappa/2$) [70], and the system reaches its steady state when $t \to \infty$. At $\phi = -\pi/2$, the quadrature X_{in} (Y_{in}) is amplified (attenuated) as

$$\frac{\langle X_{\text{out}}\rangle}{\langle X_{\text{in}}\rangle} = G, \quad \frac{\langle Y_{\text{out}}\rangle}{\langle Y_{\text{in}}\rangle} = \frac{1}{G}, \quad \text{(B10a)}$$

$$G = \left|\frac{4|\alpha| + \kappa}{4|\alpha| - \kappa}\right|. \quad \text{(B10b)}$$

Therefore, the dynamics in Eq. (B7) causes one signal quadrature of the input field to be amplified while the conjugate one to be attenuated. Since the commutation relation is preserved, no extra noise is introduced in principle [61]. In the numerical calculations in Fig. 3 in the main article, we set $\langle c_{\text{in}}\rangle$ as a real number. Moreover, if we consider that ϕ is shifted away from $\pi/2$, the gain now becomes dependent on the phase ϕ, which is shown in Eq. (30). We assumed that the input signal is much weaker compared to the amplified strength, i.e., $\sqrt{\kappa}\langle c_{\text{in}}\rangle \ll |\alpha|$. In the steady state, the phonon number inside the SAW resonator is [70]

$$N = \langle b^\dagger b\rangle = \frac{8|\alpha|^2}{\kappa^2 - 16|\alpha|^2}. \quad \text{(B11)}$$

In an ideal MPA case, $4|\alpha|$ can approach κ with a very small deviation. As a result, the steady-state phonon number can be ultralarge when $4|\alpha| \simeq \kappa$. However, our proposal is based on an UOM system mediated by a qubit. As shown in Eq. (B9), during the amplifying process, the qubit-induced Kerr nonlinearity sets a limitation on the phonon number. Moreover, when deriving Hamiltonian (B3), we assumed that the qubit is approximately in its ground state. When N is too large, the qubit can be effectively excited. The derivation given in Sec. I is not valid any more. We should make sure that our proposal is in the quasidispersive regime [65], i.e., $N < \omega_q^2/(4g_x^2)$. As a result, the critical phonon number should satisfy

$$N_c = \max\left\{\frac{\Omega_d\omega_q}{g_x^2}, \frac{\omega_q^2}{4g_x^2}\right\}. \quad \text{(B12)}$$

The UOM system can work as an effective MPA below the critical phonon number N_c. Therefore, the amplitude $|\alpha|$ should satisfy

$$4|\alpha| < \kappa\sqrt{2N_c/(2N_c + 1)}, \quad \text{(B13)}$$

which consequently leads to a critical maximum gain in Eq. (31), which is valid when $N_c \gg 1$. Thus, the maximum mechanical amplification gain is bounded by G_c.

[1] W. P. Bowen and G. J. Milburn, *Quantum Optomechanics* (CRC Press, Boca Raton, FL, 2015).

[2] M. Aspelmeyer, T. J. Kippenberg, and F. Marquardt, *Cavity Optomechanics: Nano- and Micromechanical Resonators Interacting with Light* (Springer, New York, 2014).

[3] C. K. Law, Interaction between a moving mirror and radiation pressure: A Hamiltonian formulation, Phys. Rev. A **51**, 2537 (1995).

[4] S. Bose, K. Jacobs, and P. L. Knight, Preparation of nonclassical states in cavities with a moving mirror, Phys. Rev. A **56**, 4175 (1997).

[5] A. Bassi, K. Lochan, S. Satin, T. P. Singh, and H. Ulbricht, Models of wave-function collapse, underlying theories, and experimental tests, Rev. Mod. Phys. **85**, 471 (2013).

[6] M. P. Blencowe, Effective Field Theory Approach to Gravitationally Induced Decoherence, Phys. Rev. Lett. **111**, 021302 (2013).

[7] G. Schaller, R. Schützhold, G. Plunien, and G. Soff, Dynamical Casimir effect in a leaky cavity at finite temperature, Phys. Rev. A **66**, 023812 (2002).

[8] W.-J. Kim, J. H. Brownell, and R. Onofrio, Detectability of Dissipative Motion in Quantum Vacuum Via Superradiance, Phys. Rev. Lett. **96**, 200402 (2006).

[9] J. R. Johansson, G. Johansson, C. M. Wilson, and F. Nori, Dynamical Casimir Effect in a Superconducting Coplanar Waveguide, Phys. Rev. Lett. **103**, 147003 (2009).

[10] C. M. Wilson, G. Johansson, A. Pourkabirian, M. Simoen, J. R. Johansson, T. Duty, F. Nori, and P. Delsing, Observation of the dynamical Casimir effect in a superconducting circuit, Nature (London) **479**, 376 (2011).

[11] P. D. Nation, J. R. Johansson, M. P. Blencowe, and F. Nori, Colloquium: Stimulating uncertainty: Amplifying the quantum vacuum with superconducting circuits, Rev. Mod. Phys. **84**, 1 (2012).

[12] J. R. Johansson, G. Johansson, C. M. Wilson, P. Delsing, and F. Nori, Nonclassical microwave radiation from the dynamical Casimir effect, Phys. Rev. A **87**, 043804 (2013).

[13] V. Macrì, A. Ridolfo, O. Di Stefano, A. F. Kockum, F. Nori, and S. Savasta, Nonperturbative Dynamical Casimir Effect in Optomechanical Systems: Vacuum Casimir-Rabi Splittings, Phys. Rev. X **8**, 011031 (2018).

[14] O. Di Stefano, A. Settineri, V. Macrì, A. Ridolfo, R. Stassi, A. F. Kockum, S. Savasta, and F. Nori, Interaction of Mechanical Oscillators Mediated by the Exchange of Virtual Photon Pairs, Phys. Rev. Lett. **122**, 030402 (2019).

[15] W. Marshall, C. Simon, R. Penrose, and D. Bouwmeester, Towards Quantum Superpositions of a Mirror, Phys. Rev. Lett. **91**, 130401 (2003).

[16] J.-Q. Liao and L. Tian, Macroscopic Quantum Superposition in Cavity Optomechanics, Phys. Rev. Lett. **116**, 163602 (2016).

[17] I. Carusotto, R. Balbinot, A. Fabbri, and A. Recati, Density correlations and analog dynamical Casimir emission of Bogoliubov phonons in modulated atomic Bose-Einstein condensates, Eur. Phys. J. D **56**, 391 (2009).

[18] D. Boiron, A. Fabbri, P.-É. Larré, N. Pavloff, C. I. Westbrook, and P. Ziń, Quantum Signature of Analog Hawking Radiation in Momentum Space, Phys. Rev. Lett. **115**, 025301 (2015).

[19] S. Eckel, A. Kumar, T. Jacobson, I. B. Spielman, and G. K. Campbell, A Rapidly Expanding Bose-Einstein Condensate: An Expanding Universe in the Lab, Phys. Rev. X **8**, 021021 (2018).

[20] R. P. Schmit, B. G. Taketani, and F. K. Wilhelm, Quantum simulation of Hawking radiation with surface acoustic waves, arXiv:1804.04092.

[21] D. Rugar and P. Grütter, Mechanical Parametric Amplification and Thermomechanical Noise Squeezing, Phys. Rev. Lett. **67**, 699 (1991).

[22] D. W. Carr, S. Evoy, L. Sekaric, H. G. Craighead, and J. M. Parpia, Parametric amplification in a torsional microresonator, Appl. Phys. Lett. **77**, 1545 (2000).

[23] M. Zalalutdinov, A. Olkhovets, A. Zehnder, B. Ilic, D. Czaplewski, H. G. Craighead, and J. M. Parpia, Optically pumped parametric amplification for micromechanical oscillators, Appl. Phys. Lett. **78**, 3142 (2001).

[24] R. B. Karabalin, S. C. Masmanidis, and M. L. Roukes, Efficient parametric amplification in high and very high frequency piezoelectric nanoelectromechanical systems, Appl. Phys. Lett. **97**, 183101 (2010).

[25] X. Gu, A. F. Kockum, A. Miranowicz, Y.-X. Liu, and F. Nori, Microwave photonics with superconducting quantum circuits, Phys. Rep. **718-719**, 1 (2017).

[26] J. D. Thompson, B. M. Zwickl, A. M. Jayich, F. Marquardt, S. M. Girvin, and J. G. E. Harris, Strong dispersive coupling of a high-finesse cavity to a micromechanical membrane, Nature (London) **452**, 72 (2008).

[27] D. E. Bruschi and A. Xuereb, Mechano-optics: an optomechanical quantum simulator, New J. Phys. **20**, 065004 (2018).

[28] M. Aspelmeyer, T. J. Kippenberg, and F. Marquardt, Cavity optomechanics, Rev. Mod. Phys. **86**, 1391 (2014).

[29] A. F. Kockum, A. Miranowicz, S. De Liberato, S. Savasta, and F. Nori, Ultrastrong coupling between light and matter, Nat. Rev. Phys. **1**, 19 (2019).

[30] T. T. Heikkilä, F. Massel, J. Tuorila, R. Khan, and M. A. Sillanpää, Enhancing Optomechanical Coupling via the Josephson Effect, Phys. Rev. Lett. **112**, 203603 (2014).

[31] J.-M. Pirkkalainen, S. U. Cho, F. Massel, J. Tuorila, T. T. Heikkilä, P. J. Hakonen, and M. A. Sillanpää, Cavity optomechanics mediated by a quantum two-level system, Nat. Commun. **6**, 6981 (2015).

[32] Y. J. Zhao, Y. L. Liu, Y. X. Liu, and F. Nori, Generating nonclassical photon states via longitudinal couplings between superconducting qubits and microwave fields, Phys. Rev. A **91**, 053820 (2015).

[33] S. Richer and D. DiVincenzo, Circuit design implementing longitudinal coupling: A scalable scheme for superconducting qubits, Phys. Rev. B **93**, 134501 (2016).

[34] S. Richer, N. Maleeva, S. T. Skacel, I. M. Pop, and D. DiVincenzo, Inductively shunted transmon qubit with tunable transverse and longitudinal coupling, Phys. Rev. B **96**, 174520 (2017).

[35] D. Zueco, G. M. Reuther, S. Kohler, and P. Hänggi, Qubit-oscillator dynamics in the dispersive regime: Analytical theory beyond the rotating-wave approximation, Phys. Rev. A **80**, 033846 (2009).

[36] N. Didier, J. Bourassa, and A. Blais, Fast Quantum Non-demolition Readout by Parametric Modulation of Longitudinal Qubit-Oscillator Interaction, Phys. Rev. Lett. **115**, 203601 (2015).

[37] M. Cirio, K. Debnath, N. Lambert, and F. Nori, Amplified Optomechanical Transduction of Virtual Radiation Pressure, Phys. Rev. Lett. **119**, 053601 (2017).

[38] P. Rabl, P. Cappellaro, M. V. Gurudev Dutt, L. Jiang, J. R. Maze, and M. D. Lukin, Strong magnetic coupling between an electronic spin qubit and a mechanical resonator, Phys. Rev. B **79**, 041302(R) (2009).

[39] M. Poot, S. Etaki, I. Mahboob, K. Onomitsu, H. Yamaguchi, Ya. M. Blanter, and H. S. J. van der Zant, Tunable Backaction of a DC SQUID on an Integrated Micromechanical Resonator, Phys. Rev. Lett. **105**, 207203 (2010).

[40] J. D. Teufel, T. Donner, D.-L. Li, J.-W. Harlow, M. S. Allman, K. Cicak, A. J. Sirois, J. D. Whittaker, K. W. Lehnert, and R. W. Simmonds, Sideband cooling of micromechanical motion to the quantum ground state, Nature (London) **475**, 359 (2011).

[41] J. J. Viennot, X. Ma, and K. W. Lehnert, Phonon-Number-Sensitive Electromechanics, Phys. Rev. Lett. **121**, 183601 (2018).

[42] R. Manenti, M. J. Peterer, A. Nersisyan, E. B. Magnusson, A. Patterson, and P. J. Leek, Surface acoustic wave resonators in the quantum regime, Phys. Rev. B **93**, 041411(R) (2016).

[43] R. Manenti, A. F. Kockum, A. Patterson, T. Behrle, J. Rahamim, G. Tancredi, F. Nori, and P. J. Leek, Circuit quantum acousto-dynamics with surface acoustic waves, Nat. Commun. **8**, 975 (2017).

[44] M. V. Gustafsson, T. Aref, A. F. Kockum, M. K. Ekstrom, G. Johansson, and P. Delsing, Propagating phonons coupled to an artificial atom, Science **346**, 207 (2014).

[45] P. Delsing *et al.*, The 2019 surface acoustic waves roadmap, J. Phys. D **52**, 353001 (2019).

[46] A. F. Kockum, G. Johansson, and F. Nori, Decoherence-Free Interaction Between Giant Atoms in Waveguide Quantum Electrodynamics, Phys. Rev. Lett. **120**, 140404 (2018).

[47] M. J. A. Schuetz, E. M. Kessler, G. Giedke, L. M. K. Vandersypen, M. D. Lukin, and J. I. Cirac, Universal Quantum Transducers Based on Surface Acoustic Waves, Phys. Rev. X **5**, 031031 (2015).

[48] A. N. Bolgar, J. I. Zotova, D. D. Kirichenko, I. S. Besedin, A. V. Semenov, R. S. Shaikhaidarov, and O. V. Astafiev, Quantum Regime of a Two-Dimensional Phonon Cavity, Phys. Rev. Lett. **120**, 223603 (2018).

[49] J. Q. You and F. Nori, Quantum information processing with superconducting qubits in a microwave field, Phys. Rev. B **68**, 064509 (2003).

[50] E. K. Irish and K. Schwab, Quantum measurement of a coupled nanomechanical resonator–Cooper-pair box system, Phys. Rev. B **68**, 155311 (2003).

[51] C. P. Sun, L. F. Wei, Yu-xi Liu, and F. Nori, Quantum transducers: Integrating transmission lines and nanomechanical resonators via charge qubits, Phys. Rev. A **73**, 022318 (2006).

[52] E. A. Sete, J. M. Martinis, and A. N. Korotkov, Quantum theory of a bandpass Purcell filter for qubit readout, Phys. Rev. A **92**, 012325 (2015).

[53] E. Sánchez-Burillo, L. Martín-Moreno, J. J. García-Ripoll, and D. Zueco, Full two-photon down-conversion of a single photon, Phys. Rev. A **94**, 053814 (2016).

[54] J. R. Johansson, P. D. Nation, and F. Nori, Qutip 2: A Python framework for the dynamics of open quantum systems, Comput. Phys. Commun. **184**, 1234 (2013).

[55] J. R. Johansson, P. D. Nation, and F. Nori, Qutip: An open-source Python framework for the dynamics of open quantum systems, Comput. Phys. Commun. **183**, 1760 (2012).

[56] J. C. Sankey, C. Yang, B. M. Zwickl, A. M. Jayich, and J. G. E. Harris, Strong and tunable nonlinear optomechanical coupling in a low-loss system, Nat. Phys. **6**, 707 (2010).

[57] J.-Q. Liao and F. Nori, Single-photon quadratic optomechanics, Sci. Rep. **4**, 6302 (2014).

[58] A. Nunnenkamp, K. Børkje, J. G. E. Harris, and S. M. Girvin, Cooling and squeezing via quadratic optomechanical coupling, Phys. Rev. A **82**, 021806(R) (2010).

[59] H.-T. Tan, F. Bariani, G.-X. Li, and P. Meystre, Generation of macroscopic quantum superpositions of optomechanical oscillators by dissipation, Phys. Rev. A **88**, 023817 (2013).

[60] J.-Q. Liao and F. Nori, Photon blockade in quadratically coupled optomechanical systems, Phys. Rev. A **88**, 023853 (2013).

[61] C. M. Caves, Quantum limits on noise in linear amplifiers, Phys. Rev. D **26**, 1817 (1982).

[62] A. A. Clerk, M. H. Devoret, S. M. Girvin, F. Marquardt, and R. J. Schoelkopf, Introduction to quantum noise, measurement, and amplification, Rev. Mod. Phys. **82**, 1155 (2010).

[63] A. Blais, R.-S. Huang, A. Wallraff, S. M. Girvin, and R. J. Schoelkopf, Cavity quantum electrodynamics for superconducting electrical circuits: An architecture for quantum computation, Phys. Rev. A **69**, 062320 (2004).

[64] M. Boissonneault, J. M. Gambetta, and A. Blais, Nonlinear dispersive regime of cavity QED: The dressed dephasing model, Phys. Rev. A **77**, 060305(R) (2008).

[65] M. Boissonneault, J. M. Gambetta, and A. Blais, Dispersive regime of circuit QED: Photon-dependent qubit dephasing and relaxation rates, Phys. Rev. A **79**, 013819 (2009).

[66] J.-C. Jaskula, G. B. Partridge, M. Bonneau, R. Lopes, J. Ruaudel, D. Boiron, and C. I. Westbrook, Acoustic Analog to the Dynamical Casimir Effect in a Bose-Einstein Condensate, Phys. Rev. Lett. **109**, 220401 (2012).

[67] A. Motazedifard, M. H. Naderi, and R. Roknizadeh, Dynamical Casimir effect of phonon excitation in the dispersive regime of cavity optomechanics, J. Opt. Soc. Am. B **34**, 642 (2017).

[68] J. R. Johansson, G. Johansson, C. M. Wilson, and F. Nori, Dynamical Casimir effect in superconducting microwave circuits, Phys. Rev. A **82**, 052509 (2010).

[69] Y.-X. Liu, A. Miranowicz, Y. B. Gao, J. Bajer, C. P. Sun, and F. Nori, Qubit-induced phonon blockade as a signature of quantum behavior in nanomechanical resonators, Phys. Rev. A **82**, 032101 (2010).

[70] M. O. Scully and M. S. Zubairy, *Quantum Optics* (Cambridge University Press, Cambridge, England, 1997).

[71] P. Lähteenmäki, G. S. Paraoanu, J. Hassel, and P. J. Hakonen, Dynamical Casimir effect in a Josephson metamaterial, Proc. Natl. Acad. Sci. USA **110**, 4234 (2013).

[72] A. Lambrecht, M.-T. Jaekel, and S. Reynaud, Motion Induced Radiation from a Vibrating Cavity, Phys. Rev. Lett. **77**, 615 (1996).

[73] K. J. Satzinger, Y. P. Zhong, H. S. Chang, G. A. Peairs, A. Bienfait, Ming-Han Chou, A. Y. Cleland, C. R. Conner, É. Dumur, J. Grebel, I. Gutierrez, B. H. November, R. G. Povey, S. J. Whiteley, D. D. Awschalom, D. I. Schuster, and A. N. Cleland, Quantum control of surface acoustic-wave phonons, Nature (London) **563**, 661 (2018).

[74] A. F. Kockum, P. Delsing, and G. Johansson, Designing frequency-dependent relaxation rates and Lamb shifts for a giant artificial atom, Phys. Rev. A **90**, 013837 (2014).

[75] Y.-X. Liu, C.-X. Yang, H.-C. Sun, and X.-B. Wang, Coexistence of single- and multi-photon processes due to longitudinal couplings between superconducting flux qubits and external fields, New J. Phys. **16**, 015031 (2014).

[76] S.-Q. Ding, G. Maslennikov, R. Hablützel, and D. Matsukevich, Cross-Kerr Nonlinearity for Phonon Counting, Phys. Rev. Lett. **119**, 193602 (2017).

[77] W. J. Munro, K. Nemoto, R. G. Beausoleil, and T. P. Spiller, High-efficiency quantum-nondemolition single-photon-number-resolving detector, Phys. Rev. A **71**, 033819 (2005).